

The characteristics of two-blade Submersible Mixers' flow field inner the pool

Abstract: To study the flow pattern of submersible mixers inner the pool, the research uses FLUENT6.3 mainframe computational fluid mechanics software as well as RNG $k-\epsilon$ turbulent model, SIMPLE algorithm and rigid-lid assumption to numerically simulate the two-blade submersible mixers inner the sewage treatment pool and also analyzes the velocity distribution inner big pool and the distributions of the flow field, pressure and the velocity circulation inner the mixers' impellers. The results indicate that the fluid flow inner the pool belongs to high Reynolds number with large turbulence intensity; the fluid flow is complex, and there exists obvious big vortex; Coanda Effect and boundary-layer separation is also apparent. Clearly large vortex exists and the flow velocity near the blades is higher while the flow velocity of the pool's surface and bottom takes the form of double parabolic distribution and is lower. The velocity gradient and pressure gradient are obvious from working face to the blade back; the flow velocity is lower and the pressure is higher near the working face of the blades, moreover, there are high velocity zone and negative zone in the blade back. The velocity in the axis surface inlet and outlet the blades is also parabolic distributed, and its circulation does not vary considerably; the velocity in the axis surface inlet and outlet the blades is distributed similar as the velocity in the isometric axis surface, and its velocity circulation follows a linear law distribution. It can guide submersible mixer hydraulic performance in design study, simulation and engineering application.

Streszczenie. W artykule przedstawiono wyniki badań dotyczących przepływu w mieszaczach zatopialnych, znajdujących się w basenie. W celu przeprowadzenia symulacji mieszacza dwułopatowego, wykorzystano m. in. oprogramowanie FLUENT6.3, model turbulencji $k-\epsilon$, algorytm SIMPLE oraz założono sztywność wieka. Analizie poddano także rozkład prędkości i ciśnienia wokół wirnika mieszacza. Wyniki badań zostały omówione i przedstawione wnioski (**Charakterystyka pola przepływu w basenie z mieszaczem dwułopatowym**)

Keywords: Submersible mixer, Coanda Effect, Vortex, Rigid-lid assumption, Velocity circulation

Słowa kluczowe: mieszacz zatopialny, efekt Coandy, Vortex, prędkość wirowania

1 Introduction

With the socialization and modernization in China, the discharge of sewage increases in both rural and urban areas, which has aroused the great awareness of the government. As an important sewage treatment machinery, submersible mixers are widely applied to the urban and rural sewage treatment farm, and can be adopted in biochemical reaction pool such as anaerobic pool, sedimentation pool, aeration pool and so on[1-2].

At present, there is rare report about the research to submersible mixers and pool inner flow field at home and abroad. This article uses computational fluid mechanics software Fluent 6.3 to three dimensionally stimulates the flow field in the sewage treatment pool of two-blade submersible mixers. The research analyzes the velocity field and pressure field inner the pool and mixer, which comes to a conclusion of the characteristics, phenomenon and law of this submersible mixer inner the pool flow field.

2 Fluid Characteristics Analysis

Reynolds number is a dimensionless number to measure the relative strength of inertia force and viscous force. Higher the Reynolds number presents the inertia force plays a more important role than the viscous force, when the inertial force takes the leading role; the turbulence becomes more intense [9-12]. The equation of blender machinery for the Reynolds number is

$$(1) \quad Re = D^2 n \rho / \mu$$

Where D is the diameter of blender impeller, m; n is the speed, r/min; ρ is the density of the liquid, kg/m³; μ is the dynamic viscosity, pa·s.

Average Reynolds number of fluid in the pool $Re = dv/v$, d is the equivalent diameter, m; v is the average velocity on section, m/s; ν is kinematic viscosity [7-12], m²s⁻¹.

Turbulence intensity equals the proportion of turbulent fluctuation velocity to average velocity, and is the relative index to measure the turbulence strength, equals to $I = 0.16 Re^{-1/8}$. The greater the turbulence intensity is, the more confusion the fluid at the outlet section of the jet will be, jet

and ambient medium flow infiltration intensity is larger, leading to the larger diffusion angle. When $I < 0.01$ is the low turbulence intensity, while $I > 0.1$ is the high turbulence intensity [7-12].

Select 10 paragraphs from the underwater blenders which are widely used at present in our country, the diameters of these 10 paragraphs of underwater blenders range from 180mm to 620mm, the speeds range from /min to 480r/min. Under the required conditions of the blender, the Reynolds number of fluid and turbulence intensity of the impeller and the nearby are as shown in Table 1, Reynolds number is above 4.5×10^7 , turbulence intensity is 0.014~0.02, thus the fluid in impellers and around the impellers belongs to the fluid of medium turbulence intensity of high Reynolds number, turbulence at the outlet and inlet of the impeller is very strenuous, and fluid is in disorder.

Tab.1 Turbulence intensity and Reynolds number near the impeller

Impeller diameter/mm	Rotational speed/(r/min)	reynolds number	turbulence intensity
180	1410	45684000	0.017646
210	1400	61740000	0.016994
260	680	45968000	0.017632
320	680	69632000	0.016741
368	680	92088320	0.016166
400	740	118400000	0.015666
450	710	143775000	0.01529
460	720	152352000	0.01518
580	480	161472000	0.01507
620	480	184512000	0.014821

3 Research Object

In order to further research, this paper selects a mixer and a matched pool, and simulates this pool which the submersible mixer is stirring in. The design parameters of the submersible mixer are as follows: D=210mm, dh=70mm, n=1400r/min. The fluid is the water with the temperature of 25°C and the normal pressure. The turbulence intensity of the water in and around the impeller region is 0.017 and the Reynolds number is 6.17×10^7 which belongs to the fluid of high turbulence intensity and

Reynolds number. Generally the pool of the submersible mixer is larger, while the pool of this paper belongs to the Long and narrow pool, and the Length × width × height is 4 000mm×1 600mm×2 000mm , fluid Pool The average speed and Reynolds number of the fluid in the pool is 0.3m/s and 7x 105 which belongs to the turbulent flow.



a)

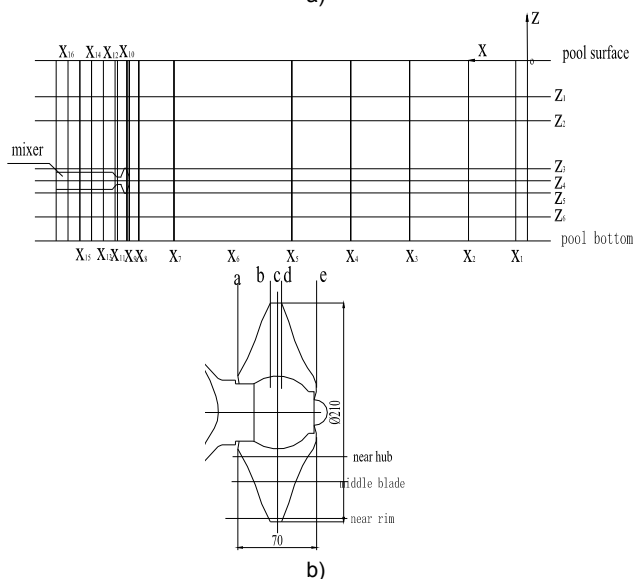


Fig.2. Pool and impeller

4 Brief Introduction of the Numerical Simulation Method

4.1 Fundamental equation

Governing equations of CFD analysis include: continuity equation, momentum equation and RNG $k - \epsilon$ turbulence equation. For the fluid that cannot be compressed, its general expression is:

$$(2) \quad \frac{\partial u_j}{\partial x_j} = 0$$

$$(3) \quad \rho \frac{\partial u_i}{\partial t} + u_j \rho \frac{\partial u_i}{\partial x_j} = -\frac{\partial p}{\partial x_i} + \mu \frac{\partial^2 u_i}{\partial x_j^2} + \rho f_i$$

$$(4) \quad \frac{\partial(\rho k)}{\partial t} + \frac{\partial(\rho k u_i)}{\partial x_i} = \frac{\partial}{\partial x_i} \left[\alpha_k \mu \frac{\partial k}{\partial x_j} \right] + G_k + \rho \epsilon$$

$$(5) \quad \frac{\partial(\rho \epsilon)}{\partial t} + \frac{\partial(\rho \epsilon u_i)}{\partial x_i} = \frac{\partial}{\partial x_i} \left[\alpha_\epsilon \mu \frac{\partial \epsilon}{\partial x_j} \right] + \frac{C_{1\epsilon}}{k} G_k - C_{2\epsilon} \rho \frac{\epsilon^2}{k}$$

In the expression, $i, j=1,2,3$; $\rho \frac{\partial u_i}{\partial t}$ is non-constant;

$u_j \frac{\partial u_i}{\partial x_j}$ is convection; $\mu \frac{\partial^2 u_i}{\partial x_j^2}$ is diffusion; ρf_i is volume

force; $C_{1\epsilon} = 1.42$; $C_{2\epsilon} = 1.68$; k is turbulence power; ϵ is dissipation rate[2-7].

4.2 Grid Segmentation

When the two-blade submersible mixers are in the pool, blades driven by the motor stir the fluid and flow the whole fluid in the pool. GAMBIT software is used to segment the grid and the grid for calculation is tetrahedral structured grid [2-7], which encrypts partly beside the stirring blades. The total number is 3857193.

4.3 Boundary condition

Because the surface of the sewage treatment pool is relatively steady and rather fluctuant free surface, rigidity cover assumption is used approximately to simulate. Suppose the normal velocity of its free surface is zero and the normal grad of each characteristic quantity is also zero, and the position of the free surface no longer changes with the time, hence grid segmentation and calculation could be worked out.

$$(6) \quad v \Big|_{z=1} = 0$$

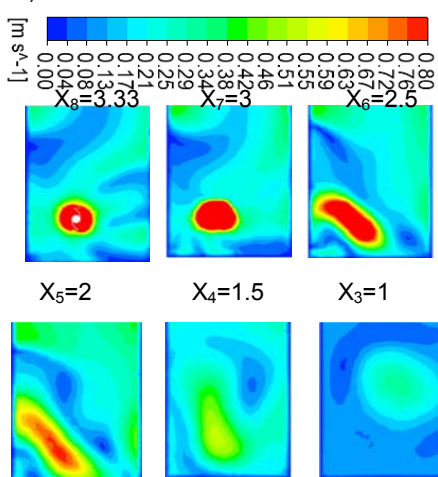
$$(7) \quad \frac{\partial q}{\partial y} \Big|_{z=1} = 0$$

With the assistance of FLUENT fluid mechanics software, the finite volume discretization method as well as the SIMPLE method and RNG $k - \epsilon$ turbulence model, the research is conditioned as all the walls, stirring axis and the surface of blades are all in non-slip condition; stirring blades and stirring axis are set at the corresponding rotation velocity condition. Convergence criterion is that all the residual absolute value of all variables is less than 10^{-4} [5-16].

5 Simulations

5.1 The characteristics of the flow field inner the pool analysis

a) x-section



b) Stream line diagram

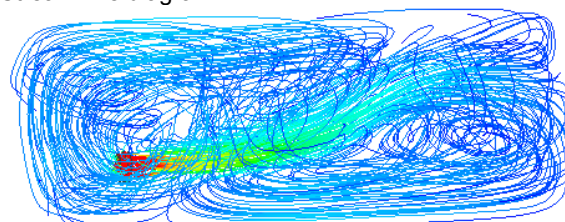


Fig.3. Velocity distribution

Figure 3 is the 3D streamline of the fluid in the pool and the velocity of the water around the submersible mixer is larger than the other of the pool. This is because the fluid that goes through the impeller can obtain great kinetic energy and form a circular momentum jet, which will jet into instationary fluid region of the pool, and what's more the fluxion of the turbulent entrains the around stationary fluid the combination of the two fluid forward movements, therefore increases the jet flow, also widens the jet width, reduces the jet velocity. Along with longer of the advance distances, the larger of the fluid obtained the kinetic energy. The fluid behind the impeller will be sucked, and obtain the kinetic energy, under the action of the pool wall. Collision and occurrence of reflux, since then, the whole pool fluid are driven, forming a large circulation, and mixing enough. Figure 3 shows that, the flow in the pool propulsion axially, radially diffusion, and the fluid circulation obviously exists several large eddies.

Fig. 4 is the fluid flow streamline diagram on two orthogonality axis. The walls are respective wall a, wall b, installation face, wall d, bottom and surface. From Fig. 4, the activity of fluid deviates the bottom and wall b. This is relevant to the installation of submersible mixer. Gernal submersible mixer is installed dissymmetrically, and near the bottom of pool. This phenomenon is called Coanda Effect, also known as wall attachment effect. Coanda Effect refers to the fact that the fluid (water or air) leaves the original flow direction, and tends to flow with the bulge on the surface. When there is skin friction between the fluid and the surface it flows, the fluid velocity will slow down. As long as the curvature of the surface is not high, according to the Bernoulli's Theorem in fluid mechanics, the decline of velocity will lead to the flow of fluid attached on the surface. Coanda Effect exists commonly in the pool with submersible mixers [7-16].

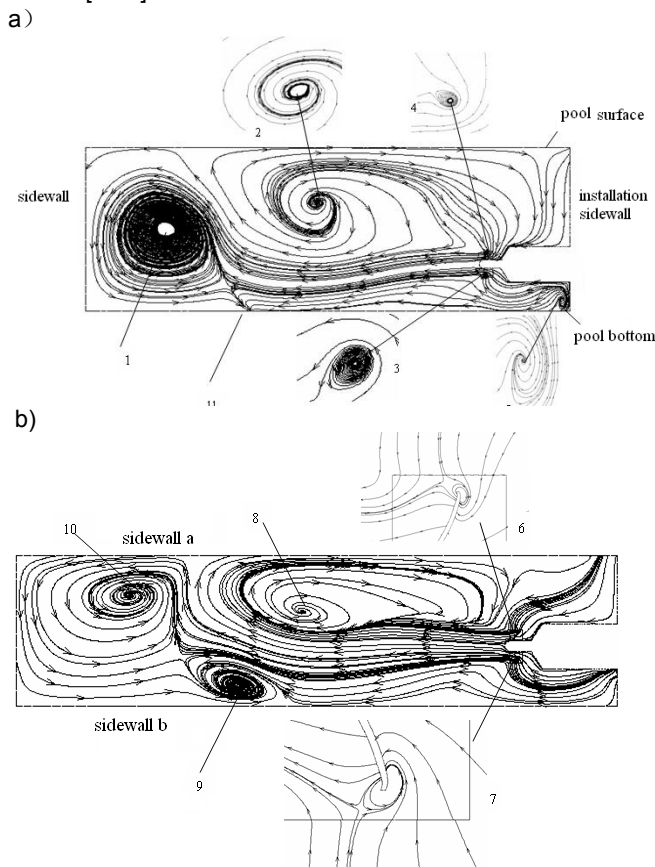


Fig.4. Streamline diagram of axial section

11 vortices can be observed in Fig. 4. No.1, No.2, No.8, No.9 and No.10 are large-sized vortex structure; No.5 is relatively smaller; No.3, No.4, No.6 and No.7 are the vortices near the blade, whose sizes are the smallest; No.11 is the large-sized vortex structure, but could still be observed. No. 2, No.4, No.6 and No.7 vortices rotate clockwise; No.1, No.3, No.5, No.6 and No.9 vortices rotate anti-clockwise. Due to the wall attachment effect, flow deviates the wall near itself. When the fluid meets the wall, the fluid will flow along the wall, and the boundary layer fluid velocity will slow down gradually and its pressure will increase. Because of the continuity of fluid, boundary layer will become thick so that more low-speed fluid can flow in at the same time. The fluid velocity decreases further and finally the kinetic energy of fluid in the entire boundary layer cannot maintain the successive flow any longer, so that the velocity in some part of the surface will be contrary to the velocity of the potential flow, so called reverse-flow. The reverse-flow will squeeze out the boundary layer to the potential flow, resulting in the sudden thickening or separation of the boundary layer. After the separation of boundary layer, it will enter the mainstream from the position closely near the surface, and will form the vortex. The large-sized vortices and many small vortices inner the pool are the results of the interaction of walls and the submersible mixer to the flow, making the interaction of wake of rotation body and boundary-layer separation on the wall, whose flow state is rather complicated.

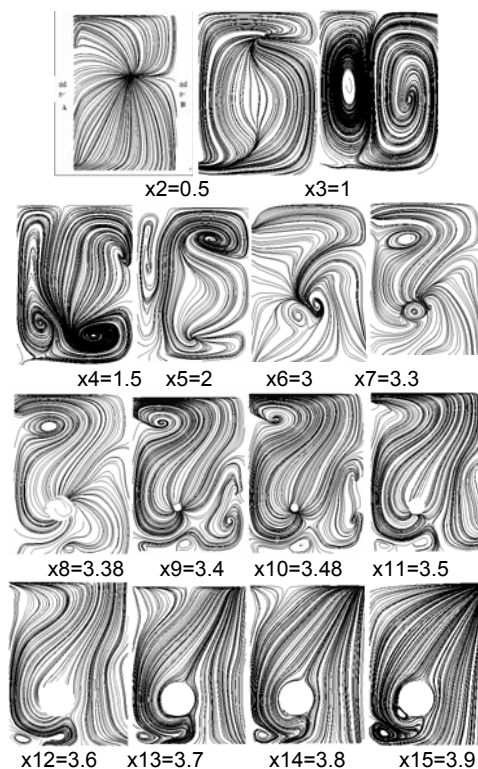


Fig.5. streamline of x-section

Fig. 2 shows the 15 sections perpendicular to the axis of submersible mixers. Suppose the wall opposite the installation wall of submersible mixer is X=0 section. These 15 sections are respectively chosen as $x_1=0.1m$, $x_2=0.5m$, $x_3=1m$, $x_4=1.5m$, $x_5=2m$, $x_6=3m$, $x_7=3.3m$, $x_8=3.38m$, $x_9=3.4m$, $x_{10}=3.48m$, $x_{11}=3.5m$, $x_{12}=3.6m$, $x_{13}=3.7m$, $x_{14}=3.8m$, $x_{15}=3.9m$. $x_8=3.38m$ is the section on the inlet of submersible mixer's impeller; $x_9=3.4m$ is the section on the stirring blade and $x_{10}=3.48m$ is the section on the outlet of the impeller. Fig. 5 is the streamline diagram of the 15 sections. The section streamlines around the impeller is

basically the same, with very obvious four big vortices. There is a vortex near the wall A, and two vortices at the bottom beside the wall B. Also there is a vortex around the bottom of pool under the installation position of submersible mixer. In the center of the pool, fluid is quite turbulent and the vortex is quite large and obvious, forming apparent back flow on all the sections. By the combined action of wall and mixer, two large vortices take their shape in $x_3=1\text{m}$. On the wall far away from the opposite submersible mixer, fluid inner the pool collides with the wall. On the sections of $x_{12}=3.6\text{m}$, $x_{13}=3.7\text{m}$, $x_{14}=3.8\text{m}$, $x_{15}=3.9\text{m}$, the fluid between the submersible mix and its installation position is quite unsteady. The vortices appear mostly on the position of wall A near the pool bottom.

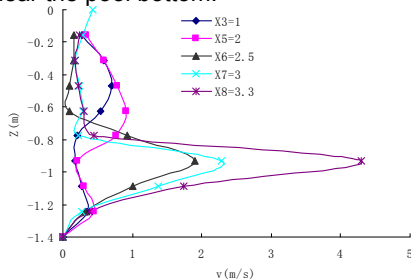


Fig.6. velocity distributions of different x line

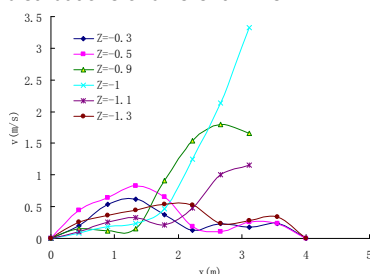


Fig. 7. Velocity distributions of different Z line

Five sections can be obtained from the intersection of sections $x_3=1\text{m}$, $x_5=2\text{m}$, $x_6=3\text{m}$, $x_7=3.3\text{m}$, $x_8=3.38\text{m}$ and $y=0$ section. Fig. 6 is the velocity diagram of the five transversals. Because it is near the impellers, affected by the rotation of impellers, the flow velocity distribution is parabola. The fluid velocity is the highest near $Z=-1\text{m}$ (the installation height of submersible mixer); the velocity does not change considerably near $Z=0\sim-0.8\text{m}$. Because the $x_3=1\text{m}$, $x_5=2\text{m}$ transversals are quite far away from the impeller, and near the wall, velocity distribution changes greatly by the co-effect of fluid and wall, and is double parabola. In the position of transversal and position opposite the axis of the installation, the value is smaller. In the $x_3=1\text{m}$ transversal, the fluid velocity achieves the maximum in $Z=-0.5\text{m}$ 与 $Z=-1.25\text{m}$; the minimum in $Z=-0.8\text{m}$. In transversal $x_5=2\text{m}$, $Z=-0.65\text{m}$ and $Z=-1.25\text{m}$, the fluid velocity achieves maximum; the minimum in $Z=-0.9\text{m}$. Six transversals can be obtained by intersection of different heights $Z_1=-0.3\text{m}$, $Z_1=-0.5\text{m}$, $Z_1=-0.9\text{m}$, $Z_1=-1\text{m}$, $Z_1=-1.1\text{m}$, $Z_1=-1.3\text{m}$ and the section $y=0$. Fig. 7 is the velocity diagram of the six transversals. $Z_1=-0.9\text{m}$, $Z_1=-1\text{m}$, $Z_1=-1.1\text{m}$ are the transversals near the axis of submersible mixer. When $x<1.5\text{m}$, flow velocity is low and smooth; when $x>1.5\text{m}$, the flow velocity gets higher and high as closer to the installation position of the mixer. While in the transversals distant from the axis, such as $Z_1=-0.3\text{m}$, $Z_1=-0.5\text{m}$, $Z_1=-1.3\text{m}$, flow velocity is double parabolic distribution—first increases and then decreases and increases and then decreases, due to the combined influence of wall, bottom and surface of the pool. There are two maximum and a minimum in every flow velocity on each transversal.

5.2 The characteristics of the flow field near the blade analysis

As is shown in Fig. 2, a、b、c、d、e five sections are selected from the inlet to outlet of blade along the axis of submersible mixer. Radial position nondimensional number r^* 's expression is

$$(8) \quad r^* = (r - r_h) / (r_l - r_h)$$

In this expression, r is measurement radius, mm; r_h is hub radius, mm; r_l is rim radius, mm.

Fig. 8 illustrates the distribution diagram of velocity on five sections of the blade. Due to the two blades, fluid inner the impeller is separated into two symmetrical parts and the flow velocity distribution is the same. The velocity in the outlet is much higher than its of the inlet, because the action of impeller to water. From the working face to the blade back, the change of flow velocity is obvious in grad. The fluid velocity is much higher in the blade back, and there exists high-speed zone; the fluid velocity near the working face is relatively low, and there is low-speed zone [18].

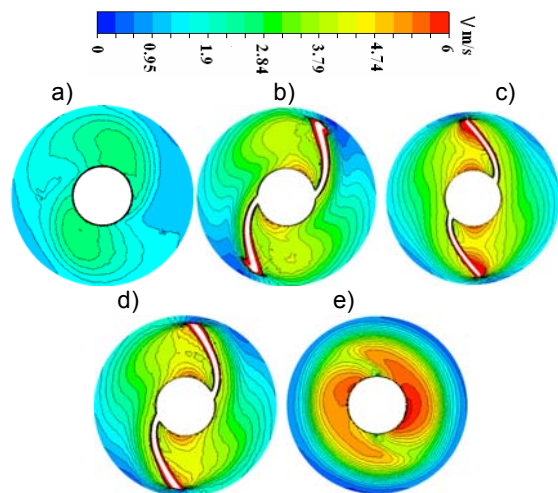


Fig.8. Velocity distribution of five sections

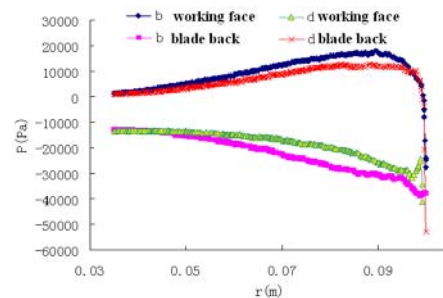


Fig.9. Static pressure distribution at impeller

Points are selected from the radius around the hub, in the center of the blades and around the rim (Fig.2). As is shown in Fig. 9, the upper static pressure distribution, the static pressure distribution trends at working face and blades back are basically the same. From the hub to the rim, as the radius increases, the static pressure at working face increases first and then decreases a little, and the negative pressure at blades back increases and then decreases as well. From the inlet to the outlet of the blades, the static pressure on the working face is smaller and smaller. The negative static pressure at the blades back is smaller and smaller too, and the pressure differential of blades is becoming smaller gradually. Because the impeller of submersible mixer is open mouthed, the pressures at working face and blades back decrease sharply, and negative pressure emerges at working face.

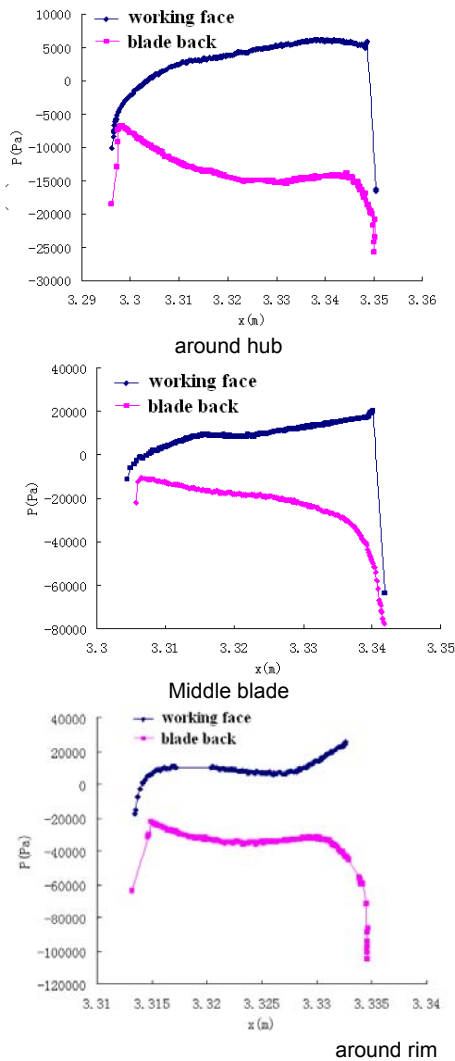


Fig.10. Static pressure distribution at blade

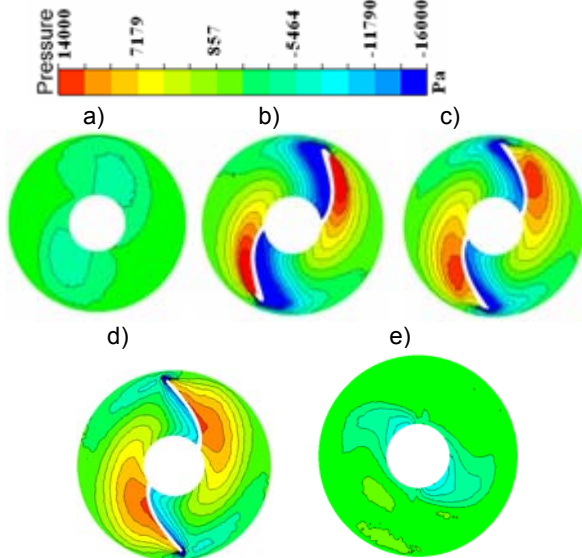


Fig.11. Static pressure distribution in impeller

Fig. 11 is the static distribution diagram of inlet and outlet on five sections. Due to non direct stirring of blades, there is slight change of static pressure from the hub to the center of section. Inside the blades, the fluid static pressure is quite high near the working face of blades, and there is

obvious high pressure zone, the fluid pressure near the blade back is very low, and forms negative pressure area. In the fluid area between the blades, the static pressure is becoming lower and lower from the working face to the blade back, and the pressure gradient is relatively obvious.

Fig.12 is the axial velocity v_{m1} 、 v_{m2} on the inlet and outlet of impeller and the circulation distribution Γ . At the inlet and outlet of impeller, the axial velocity increases first and then decreases, forming parabolic distribution. When $r^*=0.1\sim 0.6$, the velocity change is relatively smooth. Near the hub and impeller, axial velocity decreases sharply, which is probably because impeller is installed close to the electronic machine, which has big diameter, and blocks the fluid flow, leading to the low velocity near the hub. Because of the influence of blades rotation, there is velocity circulation at the outlet and inlet of the impeller; while the inlet circulation is relatively lower, changes relatively smoother, and forms the linear distribution.

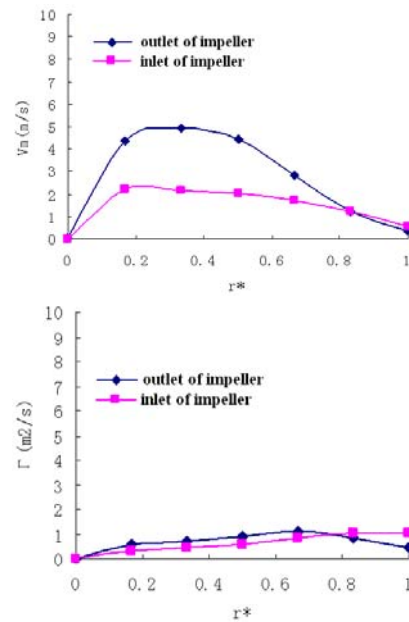


Fig.12. Axial velocity and circulation distributions at impeller inlet and outlet

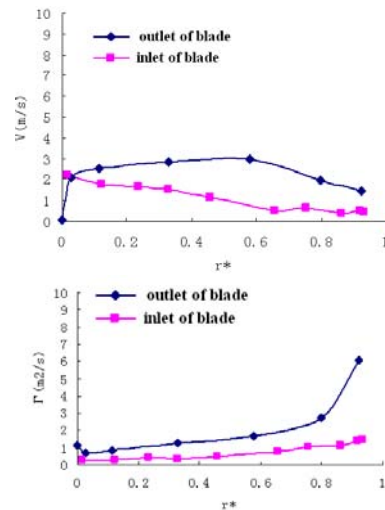


Fig.13. Axial velocity and circulation distributions at blade inlet and outlet

Fig.13 is the axial velocity v_{m1} 、 v_{m2} on the inlet and outlet of impeller and the circulation distribution Γ . The axial velocity and the velocity circulation at the outlet of blade are both higher than its at the inlet of blade. From the hub to the rim, the axial velocity at the inlet is decreasingly distributed.

Near the hub, the axial velocity at the outlet increases sharply. When $r^* > 0.05$, axial velocity at the outlet doesn't change sharply, and is distributed approximately equally. Near the rim, the axial velocity decreases slightly at the outlet of the blade. From the hub to the rim, the velocity circulation at inlet of blade forms linear distribution. Because of the boundary layer influence, the gradient of velocity circulation is relatively higher at the hub and rim area.

6 Conclusions

Combined with fluid mechanics, this article uses fluent software to numerically simulate the submersible mixer and analyze the flow field inside the pool, and finally come to the significant conclusions as follows.

1. The fluid inside the pool is high Reynolds number with high turbulence intensity.

2. The fluid inside the pool forms efflux through the impeller, propels and diffuses radially. Clearly a large vortex exists and the flow velocity near the blades is higher while the flow velocity of the pool's surface and bottom takes the form of double parabolic distribution and is lower.

3. Wall attachment effect of flow field is apparent inside the pool, where forms large vortex and Avortex, as well as many small vortices whose activity is complex. The co-effect of walls and submersible mixer to the flow makes corresponding effect of the vortices formed by the wake of rotation body and boundary-layer separation on the wall.

4. The velocity gradient and pressure gradient are obvious from working face to the blade back; the flow velocity is lower and the pressure is higher near the working face of the blades. Moreover, there are high velocity zone and negative zone in the blade back. The velocity in the axis surface inlet and outlet of the blades is also parabolic distributed, and its circulation does not vary considerably; the velocity in the axis surface inlet and outlet of the blades is distributed similar as the velocity in the isometric axis surface, and its velocity circulation follows a linear law distribution.

Acknowledgements

This work was supported by Jiangsu College graduate research and innovation projects (Grant No: CX10B_264Z), national natural science foundation (Grant No: 51109093), National Science and technology support program (Grant No: 2011BAF14B01) and production and research prospective joint research projects of Jiangsu Province (Grant No: BY2010131).

REFERENCES

- [1] XU Weixing. *Design Theory of Submersible Mixer Impeller and Numerical Simulation of Agitated Flow Field*. 2006.4-5.
- [2] WU Wei-qiang. *Introduction How to Select Mixer in Sewage Treatment Plant*. China Science and Technology Information. May.2008,116-118.
- [3] YAN Jianhua, HUANG Jiandao, TENG Guorong. *Research on Rural Domestic Sewage Disposal of Biologic Disposal High Efficiency Blender*. Journal of Anhui Agri Sci., 37 (2009), No.20, 9606 – 9607.
- [4] SHI Wei-dong, TIAN Fei. *Study on Inner Flow of New-Type Streamline XCK Mixer with Two Blades. Hydraulic influence factors and inner flow analysis of centrifugal fire pump*, 26(2008), No. 6, 6-9.

- [5] Ventikos Y, Tzabiras G. *A numerical study of the steady and unsteady cavitation phenomenon around hydrofoils*. In: CAV'95 International Conference, Deauville, France. 1995.
- [6] Spalding DB. *Numerical computation of multi-phase flows. V.K.I. for Fluid Dynamics*. Lecture Series, 1981.
- [7] Kinnas SA, Fine NE. *A numerical non-linear analysis of the flow around two- dimensional and three-dimensional partially cavitating hydrofoils*. J Fluid Mech. 254(1993), 51-81.
- [8] Li Guowei¹, Wang Yan², Lü Xiuli¹, et al. *Numerical simulation of three-dimensional flow field in centrifugal pump with deviated short splitter vanes*. Transactions of the CSAE, 27(2011), No. 7,151-155.
- [9] TIAN Fei, SHI Weidong. *Hydraulic Design and Experimental Study on the Wastewater Treatment Mixer*. FLUID MACHINERY, 39(2011), No. 6, 1-4.
- [10] TIAN Fei, SHI Weidong. *The effect of dome on wastewater-treatment mixer performance*. Journal of Engineering Thermophysics, 31(2010), 245-248.
- [11] SHI Weidong, TIAN Fei. *Flow Analysis and Measurement of Wastewater Treatment Mixer with Dome*. China Academic Journal Electronic Publishing House, 42(2011), No.3, 96-99.
- [12] SHI Wei-dong, ZHANG Qi-hua, LU Wei-gang. *Hydraulic design of new-type deep well pump and its flow calculation*. Journal of Jiang su Un iversity(Natural Science Edition. 27(2006), No. 6, 529-531.
- [13] Wang Fujun, Zhang Ling, Zhang Zhimin. *Analysis on pressure fluctuation of unsteady flow in axial flow pump*. Journal of Hydraulic Engineering, 38(2007), No. 8, 1003-1009.
- [14] L. Prandtl, K. Oswatitsch. *Prandtl's Essentials of Fluid Mechanics*. BEIJING, Aerospace Science press 1984, 75-400.
- [15] Guang Dong engineering College Group, *"Marine propeller design,"* People Traffic Press, 1976, 12-13. (in Chinese)
- [16] Wang Kai, Lv Jun. *mixing equipment*. Beijing: Chemical Industry Press,2004.
- [17] Yousefi Hassan, Noorzad Asadollah, Farjoodi Jamshid. *Multiresolution-Based Adaptive Simulation of Wave Equation*. Applied Mathematics & Information Sciences, 6(2012), No. 1, 47-58.
- [18] Koun-Tem Sun , Ching-Ling Lin, Hsin-Te Chan , Hong-Ming Kang , Man-Ting Ku, *Comparisons between the Hybrid Taguchi-Genetic Algorithm and Genetic Algorithm*, Advances in Industrial Engineering and Management, 1(2012), No.1, 10-18

Authors: Tian Fei, doctoral student, Jiangsu University, e-mail: huangzi-fei@163.com; Shi Weidong, Professor, Vice President of Jiangsu University, E-Mail: wdshi@ujs.edu.cn; Zhang Qihua, Assistant researcher, Research Center of Fluid Machinery Engineering and Technology of Jiangsu University, qihua05@163.com; Jiang Hua, Lecturer, Southeast University Chengxian College, E-Mail: 89303956@qq.com; Zhang Desheng, Assistant researcher, Research Center of Fluid Machinery Engineering and Technology of Jiangsu University, desheng1982@163.com.

The correspondence address is: 301, Xuefu Road, Zhenjiang, 212013, Jiangsu Province, P.R. China.

E-mail: wdshi@ujs.edu.cn.